C.2

NACA

RESEARCH MEMORANDUM

SCHLIEREN INVESTIGATION OF THE WING SHOCK-WAVE BOUNDARY-LAYER INTERACTION IN FLIGHT

By George E. Cooper and Richard S. Bray

Ames Aeronautical Laboratory
Moffett Field, Calif.

NATIONAL ADVISORY COMMITTEE
FOR AERONAUTICS

WASHINGTON
September 19, 1951

NATIONAL ADVISORY COMMITTEE FOR AERONAUTICS

RESEARCH MEMORANDUM

SCHLIEREN INVESTIGATION OF THE WING SHOCK-WAVE BOUNDARY-LAYER INTERACTION IN FLIGHT

By George E. Cooper and Richard S. Bray

SUMMARY

This report presents the data obtained in flight using a schlieren apparatus which photographed the shock-wave interaction with a thick turbulent boundary layer on a wing. Local Mach number and boundary-layer characteristics obtained from pressure measurements in the vicinity of the shock wave are also presented.

Good correlation with theoretical and wind-tunnel investigations of boundary-layer shock-wave interaction was obtained, particularly with respect to the lower Mach number for the establishment of a forked or bifurcated type of shock wave. The boundary layer did not appear to thicken behind the normal shock wave. Considerable thickening, associated with separation, did occur, however, with increasing Mach number after the formation of the forked shock wave.

The density gradient in the boundary layer appeared to increase markedly just behind the shock wave. This stronger gradient, however, appeared to be dissipating at approximately five to six boundary-layer thicknesses behind the shock.

INTRODUCTION

Detailed measurements of shock-wave boundary-layer interaction have been made in wind tunnels at small or moderate Reynolds number. Previous flight tests at high Reynolds number have been limited to pressure measurements. The purpose of the tests covered by this report was to investigate the region of shock-wave interaction with a thick turbulent boundary layer on a wing at full-scale flight Reynolds numbers utilizing both a schlieren apparatus and pressure measurements.

The presence of a bifurcated or forked shock wave associated with a turbulent boundary layer has been noted in the wind-tunnel investigations of Fage and Sargent in reference 1. Forked shock waves have

been treated theoretically by Weise (reference 2) and Eggink (reference 3). They independently determined the flow conditions theoretically necessary for the existence of such shock waves. They further associated this type of shock with detached or separated flow. Wuest in reference 4 verified and extended these results by a more straightforward analysis. The local Mach number ahead of the shock wave below which the forked shock could not theoretically exist was determined by Eggink, Weise, and Wuest as 1.245.

The present report is concerned with the flow conditions associated with the establishment of the forked shock wave.

SYMBOLS

H	boundary-layer shape parameter $\left(\frac{\delta^*}{\theta}\right)$
M	Mach number
R	Reynolds number based on wing section chord
R_θ	boundary-layer Reynolds number $\left(U_\delta \frac{\theta}{\nu_\delta}\right)$
c	wing section chord (84.5 in.)
p	static pressure
u	local velocity in boundary layer
x	chordwise distance
y	distance normal to wing surface
θ	boundary-layer momentum thickness $\left[\int_0^\delta \frac{\rho u}{\rho_\delta u_\delta}\left(1 - \frac{u}{u_\delta}\right)dy\right]$
δ	boundary-layer thickness
δ^*	boundary-layer displacement thickness $\left[\int_0^\delta \left(1 - \frac{\rho u}{\rho_\delta u_\delta}\right) dy\right]$
ν	kinematic viscosity
ρ	density

Subscripts

o	free-stream condition
1	local condition just ahead of shock $(\frac{x}{c} = 0.553)$
2	local condition just behind shock $(\frac{x}{c} = 0.581)$
p	measured by probe in contrast to surface orifice
δ	condition at outer edge of boundary layer

APPARATUS

Schlieren Instrument

Optics.- The optical arrangement used in the schlieren apparatus, shown in figure 1, was essentially a conventional two-lens system. A 35-mm f2.3 photographic lens was used as a condensing lens to form an image of the lamp at the slit, which was formed by razor blades, and was adjustable along, and normal to and rotatable with respect to, the optical axis. The main lenses were 3-inch-diameter achromats having a short focal length of 8 inches because of the severe space restriction imposed in mounting the instrument in the wing. The space requirements made it necessary to use three front surface one-quarter-wave-length mirrors within the instrument. (See fig. 1.) At the outset of the tests a knife edge made of a razor blade was used with only fair results. The best results and all data presented in this report were obtained by substituting for the knife edge a cut-off consisting of a section of a 200-line-per-inch photographic grid. The cut-off was provided with the same type of adjustment as the slit. The windows were of ordinary plate glass reasonably free of striae and mounted so as to compensate for nonparallelism of the faces.

Light source and power supply.- A General Electric BH-6 high-pressure mercury vapor lamp was used for the light source. For satisfactory operation this lamp should remain essentially level. In order that this condition be met during a dive, the lamp was mounted parallel to the lateral axis of the airplane. When rotation of the light-source image was necessary, it was accomplished by mirrors within the lamp housing. Cooling air for the lamp was taken from a scoop mounted on the underside of the wing. Energy for the lamp was provided by the discharge of a capacitor, which in turn was charged through a series resonant circuit. This circuit was supplied from a 2000-volt aircraft dynamotor supplied from the 28-volt system of the airplane. Flashing of the lamp was controlled by a hydrogen-thyratron tube triggered by a framing

contactor, in turn operated by the camera film drive. The thyratron tube discharged the energy-storage circuit capacitor through the BH-6 lamp, providing a light flash duration of the order of 1 microsecond.

Camera.- Photographic recording was accomplished by a specially modified 35-mm camera with the intermittent film transport action removed. The film was then driven at constant speeds and the framing accomplished by the flashing of the lamp. Speeds of 24, 48, and 96 frames per second were possible.

Structure.- To reduce the distortion effects of temperature and vibration, the main structure of the instrument was made of 1/4-inch and 3/8-inch steel plate, doweled and screwed together in a rigid semi-boxed construction.

Mounting.- The instrument was mounted in the gun compartment of the left wing of the test airplane as shown in figure 2. Shock mounts were used which allowed a slight movement of the instrument relative to the wing, but effectively reduced vibration of the instrument. The parts of the instrument projecting above the wing were enclosed in fairings which extended fore and aft to the leading and trailing edges of the wing as shown in figure 3. The windows were mounted flush with the inside of each fairing to provide a test channel with smooth walls.

Test Region

The test surface was the same as that on the normal wing except that cracks were filled and the major irregularities removed. A carborundum strip was added near the leading edge in an effort to minimize possible variations in boundary-layer and shock-wave characteristics as the test progressed. The test section was essentially two dimensional and consisted of a 10-inch channel extending from the leading to the trailing edge of the wing between the two fairings which extended 4-1/8 inches (4.88-percent wing chord) above the wing surface at their highest point.

Visual observations of the wing shock wave by the shadowgraph technique of reference 5 were used for positioning the instrument. This shock-wave location was verified from available wing-section pressure-destribution data. Subsequent observations, together with the schlieren photographs, confirmed the fact that there was little or no chordwise shift in the shock-wave position with the addition of the instrument and fairings.

Boundary-layer measurements made, but not presented herein, showed that the fairings had little effect on the flow characteristics of the

test channel. Also, the boundary-layer profile 0.75 inch from the channel wall was found to be almost identical with that at the center of the channel with the fairings present or removed.

The boundary layer on the walls may account for the presence of the apparently separate normal shock wave ahead of the forked shock noted in some pictures.

The relative chordwise locations of surface orifices, boundary-layer total-pressure rakes, static-pressure probes, and the schlieren field are shown in figure 4. The surface orifices and rakes were located midway between the fairings. The two probes were located approximately 3/4 inch on each side of the center line of the channel.

Pressure Measurements

A miniature Statham six-cell pressure pickup was used in conjunction with NACA recording galvanometers for measuring static pressures in the immediate vicinity of the shock wave. The instrument arrangement was such as to make possible simultaneous schlieren photographs of the shock wave and/or boundary layer and measurement of the static pressure immediately ahead of and behind the shock wave at both the surface and outer edge of the boundary layer. The boundary-layer measurements were made with a rake of total-pressure tubes and a 15-cell NACA photographically recording manometer.

TESTS

The tests were conducted in unaccelerated flight during dives of the test airplane which started from 30,000 feet with the records being taken at a nominal altitude of 20,000 feet. In figure 5 is shown the variation of Reynolds number with Mach number for the test altitude of 20,000 feet. The data presented are confined to flow with a turbulent boundary layer ahead of the shock wave and for a Reynolds number of about 10,000 based on the momentum thickness of the boundary layer ahead of the shock wave. All data presented were obtained with the fairings in place.

RESULTS AND DISCUSSION

The variation of local Mach numbers just ahead ($\frac{x}{c} = 0.553$) and just behind the shock wave ($\frac{x}{c} = 0.581$) is presented in figure 6 as a function of airplane Mach number. For the location ahead of the shock wave, the local Mach number obtained from a static pressure probe located

approximately at the edge of the boundary layer is compared with that determined from the static pressures obtained from the corresponding surface orifice directly below. The local Mach numbers, as determined by a static pressure probe near the edge of the boundary layer for the location behind the shock wave, are also presented. The differences in local Mach numbers, as determined from static pressures between the surface and edge of the boundary layer, ahead of the shock wave are in general agreement with the results of reference 6. Due to instrument difficulties, the surface static pressure for the region aft of the shock wave was not obtained. Measurements made later, however, by three static probes located at different heights through the boundary layer failed to show any measurable differences in static pressure at least 1 inch behind the shock wave.

The indicated rapid decrease in local Mach numbers M_1 and M_{1p} occurring at airplane Mach numbers greater than 0.685, which is shown in figure 6, is attributed to violent fluctuation of the shock wave across the pressure orifices. In cases where the shock-wave oscillation was such that it passed over a pressure orifice, the pressure record changed from a steady to a fluctuating one. For airplane Mach numbers from 0.670 to 0.675 the oscillation was confined between the fore and aft static orifice locations, while at Mach numbers greater than 0.680 the oscillation amplitude increased to the point where satisfactory pressure measurements in the immediate vicinity of the shock wave could not be obtained. For this reason, the various characteristics have been plotted against airplane Mach number, instead of the local Mach number ahead of the shock wave. Absolute accuracy of the measured Mach numbers was good only to 0.01, while the relative values of Mach number were accurate to approximately 0.001. Airplane Mach number has been shown in this report to three decimal places to correctly indicate differences in Mach number.

Distributions of Mach number through the boundary layer at 54.5- and 60.6-percent chord are presented in figure 7. Plots of Mach number at the outer edge of the boundary layer, ratio of boundary-layer displacement thickness to chord, ratio of boundary-layer momentum thickness to chord, and shape parameter versus airplane Mach number for these two chordwise stations are given in figure 8. The method described in reference 7 was used for the evaluation of boundary-layer displacement and momentum thicknesses.

Shock-Wave Properties

Schlieren photographs, which show the shock wave located within the field of view for the range of airplane Mach numbers from 0.670 to 0.692, are presented in figure 9. These show clearly the normal shock at an M_o of 0.670 and the forked shock wave at the higher Mach numbers.

A cut-off nearly vertical to the flow direction was used for these pictures to obtain the maximum contrast possible over the weaker front fork.

A sequence of camera frames taken at 96 frames per second and an airplane Mach number of 0.677 (M_{1_p} of 1.26) is shown in figure 10, illustrating the transition from a normal to a forked shock wave. These follow the shock wave through one cycle, from normal to forked and back to a normal wave. In this transitory stage, the forked wave is always farther aft than the normal one and hence the local Mach number would be expected to be somewhat higher ahead of the forked wave. It is observed in figures 9 and 10 that the local Mach number ahead of the shock wave for the establishment of the forked shock is in good agreement with the theoretical value of 1.245 given in references 2, 3 and 4.

Presented in figure 11 is an enlarged schlieren photograph of a forked shock wave obtained with a slightly different sensitivity setting than those of figures 9 and 10. Here the branching point appears in clearer detail, while the shock angles remain essentially the same as those measured in figure 9(e). No explanation is given for the additional normal shock wave visible in figure 11 except that it may be the result of interaction between the wing shock wave and the boundary layer on the channel walls and was visible only at this particular sensitivity setting.

By taking the experimental value of the local Mach number M_1 ahead of the shock and measuring the shock angles, it was possible to compute the flow through the shock in the manner of Eggink and Weise. The results of these calculations for the forked shock at an M_o of 0.685 gave very good agreement ($1/4^\circ$ in 5°) in regard to the final flow deflection angles obtained when comparing flow direction through the shock wave above and below the branching point. For airplane Mach numbers of 0.675 and 0.680, the angle of the front leg was always greater than theory allows for supersonic flow behind it so that final flow deflection angles could not be compared. For an M_o of 0.692, the branching point is so high that a measurement could not be obtained of the main shock wave above the branching point. The measured values of Mach number behind the shock wave were about 0.12 Mach number higher than the calculated value based on the measured M_{1_p} except for the forked wave at an M_o of 0.685. At this Mach number, however, the measured value was between that calculated for the regions above and below the branching point.

The lower termination point of the shock wave branches, as determined from the schlieren photographs of figure 9, presumably indicating where the local Mach number approaches unity in the boundary layer, can be seen in figure 12 to rise from the surface with increasing Mach number. Corresponding points where the Mach number is unity, as determined from the boundary-layer measurements upstream of the shock, are

also shown. It is seen that satisfactory agreement exists only for the initial shock formation, that of the normal shock for M_o of 0.670. Presumably, therefore, the measured boundary-layer characteristics ahead of the shock do not apply at the shock wave itself for the forked shock although fair agreement may exist for the normal shock wave.

Some tendency for the height of the branching point above the surface to increase with increasing Mach number can be seen from the photographs of figure 9, and this variation in the height of the branching point with airplane Mach number is also presented in figure 12. This increase is in general agreement with the results of Fage and Sargent in reference 1.

Shock-Wave Oscillation and Airplane Buffeting

Some shock-wave oscillation was present at all times. The maximum oscillation amplitude as a function of airplane Mach number is shown in figure 13. Maximum oscillation amplitude is defined as the distance between the most forward and rearward shock positions during a given run. The average amplitude was not determined because of the random nature of the oscillation but would have been much less than the maximum shown for airplane Mach numbers of 0.670 and 0.675, and slightly less for Mach numbers of 0.680 and 0.685. At 0.690 Mach number only single isolated frames could be found where the shock wave was in the field of view, and at 0.700 no shock waves could be seen at all. Airplane buffeting as noted by the pilot, the senior author, was very mild between 0.670 and 0.680 Mach numbers but increased considerably from 0.685 to 0.700. The frequency of the shock-wave oscillation could not be determined from the schlieren photographs which were taken at a camera speed of 96 frames per second.

Shock-Wave Boundary-Layer Interaction

Qualitative indications of the density gradient through the boundary layer with and without a shock wave are shown in the schlieren photographs of figure 14. The static probes were removed so as not to interfere with the boundary-layer pictures. A stronger gradient is apparently present in the presence of the shock wave and appears to be more uniform throughout the boundary layer than when the shock wave is absent. The increased density gradient, especially near the outer edge of the boundary layer, may have been due to a variation in static pressure caused by the presence of the shock wave, as mentioned by Liepmann in reference 8. Static pressure measurements, however, failed to show any significant pressure gradient at a location about 1 inch behind the shock wave. Evidence that the strong density gradient was rapidly dissipated downstream of the shock is indicated by figure 14(f). Here the oscillating shock wave has moved forward of the field of view so that

in figure 14(f) the boundary layer shown is at least five to six boundary-layer thicknesses behind the shock wave.

The boundary-layer displacement and momentum thicknesses decrease slightly with increasing airplane Mach number for the $\frac{x}{c}$ location of 0.545 (fig. 8(a)), while the shape parameter increases slightly. For the $\frac{x}{c}$ location of 0.606 (fig. 8(b)), all three parameters may be seen to increase abruptly at a Mach number corresponding approximately to the establishment of the shock wave, M_o of about 0.670. For increases in airplane Mach number beyond that associated with the formation of the forked shock wave, the increases in the parameters are even more marked. At these Mach numbers the shape parameter H increases from appromimately 1.8 to 3.0, corresponding with the values usually associated with separation or imminent separation at low speeds.

Boundary-layer thicknesses, measured from the extent of the density gradient shown in schlieren photographs and obtained from the pressure surveys, are presented in figure 15. It may be seen that the boundary-layer thicknesses determined by the two procedures are in good agreement. It may be observed that the boundary-layer thicknesses determined from the schlieren photographs increase abruptly at approximately the Mach number associated with branching of the shock wave. For increases in airplane Mach number above this value, both the boundary-layer thickness determined from the schlieren photographs and from the survey at an $\frac{x}{c}$ of 0.606, increased still further.

Local separation (which was intermittent) is observed in figure 14 at airplane Mach numbers as low as 0.675. Complete separation is indicated in the schlieren photograph of figure 14(f), which presents the boundary layer five to six boundary-layer thicknesses behind the shock wave.

CONCLUSIONS

From flight tests using a schlieren apparatus and pressure surveys to investigate shock-wave boundary-layer interaction on the wing of an airplane, the following is concluded:

1. The shock wave in conjunction with the thick turbulent boundary layer was found to be normal for local Mach numbers of approximately 1.24 or less ahead of the shock and became forked at higher Mach numbers.

2. The boundary layer appears to thicken behind the normal shock wave. Considerable thickening, associated with separation, did occur, however, with increasing Mach number after the formation of the forked shock wave.

3. Increasing the Mach number raised both the branch point of the forked shock wave and the lower extremity of the shock wave above the wing surface.

4. The density gradient in the boundary layer appeared to increase markedly just behind the shock wave. This stronger gradient, however, appeared to be dissipating at approximately five to six boundary-layer thicknesses behind the shock.

Ames Aeronautical Laboratory,
National Advisory Committee for Aeronautics
Moffett Field, Calif.

REFERENCES

1. Fage, A., and Sargent, R. F.: Shock-Wave and Boundary-Layer Phenomena Near a Flat Surface. Proceedings of the Royal Society, vol. 190, 1020, June 17, 1947.

2. Weise, A.: On the Separation of Flow Due to Compressibility Shock. NACA TM 1152, 1947.

3. Eggink: Compression Shocks of Detached Flow. NACA TM 1150, 1947.

4. Wuest. W.: The Boundary Position of the Forked Shock Wave. M.A.P. Volkenrode, VG 170(Rep. and Trans. 169), Aug. 15, 1946.

5. Cooper, George E., and Rathert, George A., Jr.: Visual Observations of the Shock Wave in Flight. NACA RM A8C25, 1948.

6. Ackeret, J., Feldman, F., and Rott, N: Investigations of Compression Shocks and Boundary Layers in Gases Moving at High Speed. NACA TM 1113, 1947.

7. Zalovcik, John A., and Luke, Ernest P.: Some Flight Measurements of Pressure-Distribution and Boundary-Layer Characteristics in the Presence of Shock. NACA RM L8C22, 1948.

8. Liepmann, Hans Wolfgang: Investigations of the Interaction of Boundary Layer and Shock Waves in Transonic Flow. USAF Technical Rep. No. 5668, 1948.

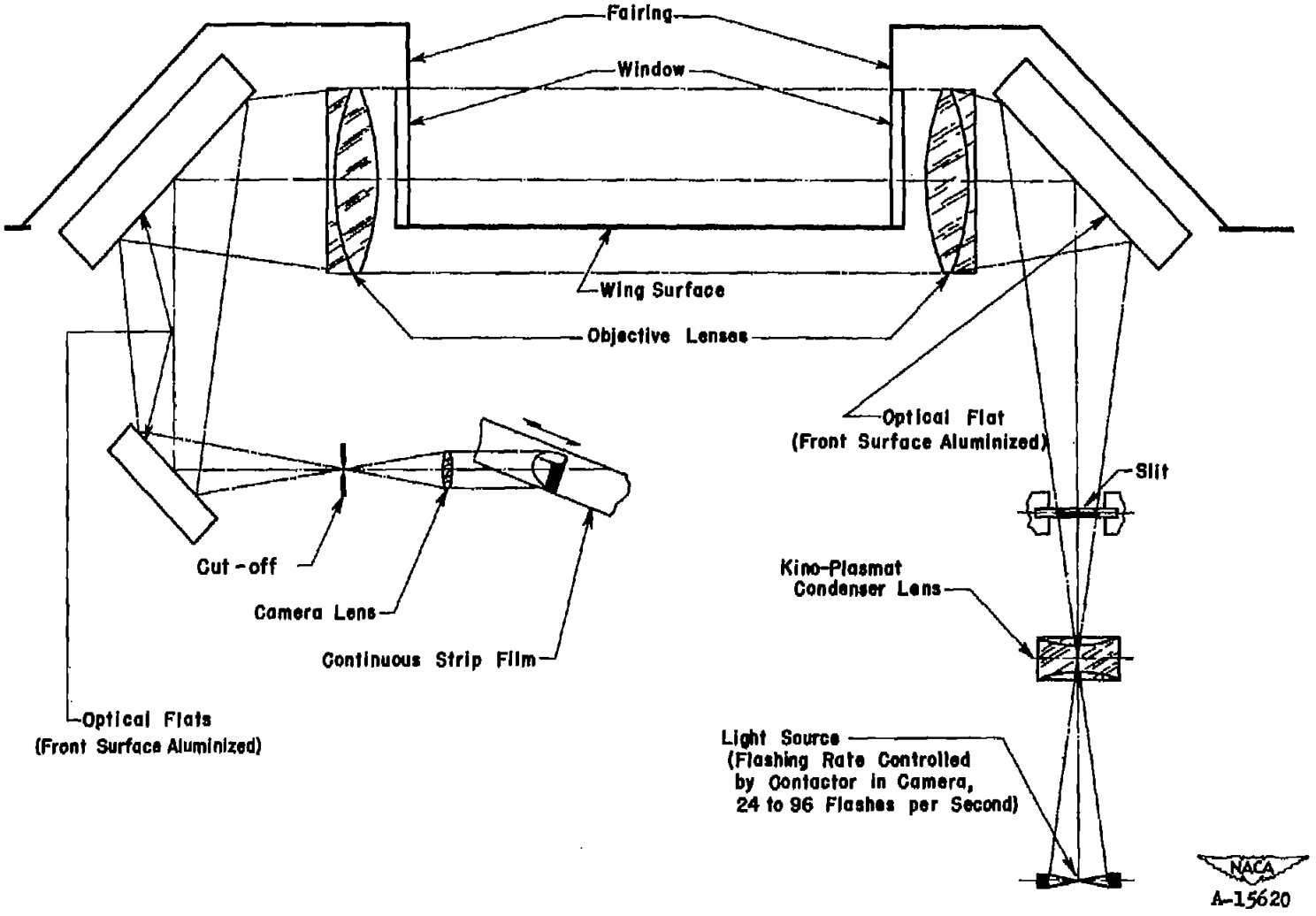

Figure 1.- Diagram of schlieren optical system.

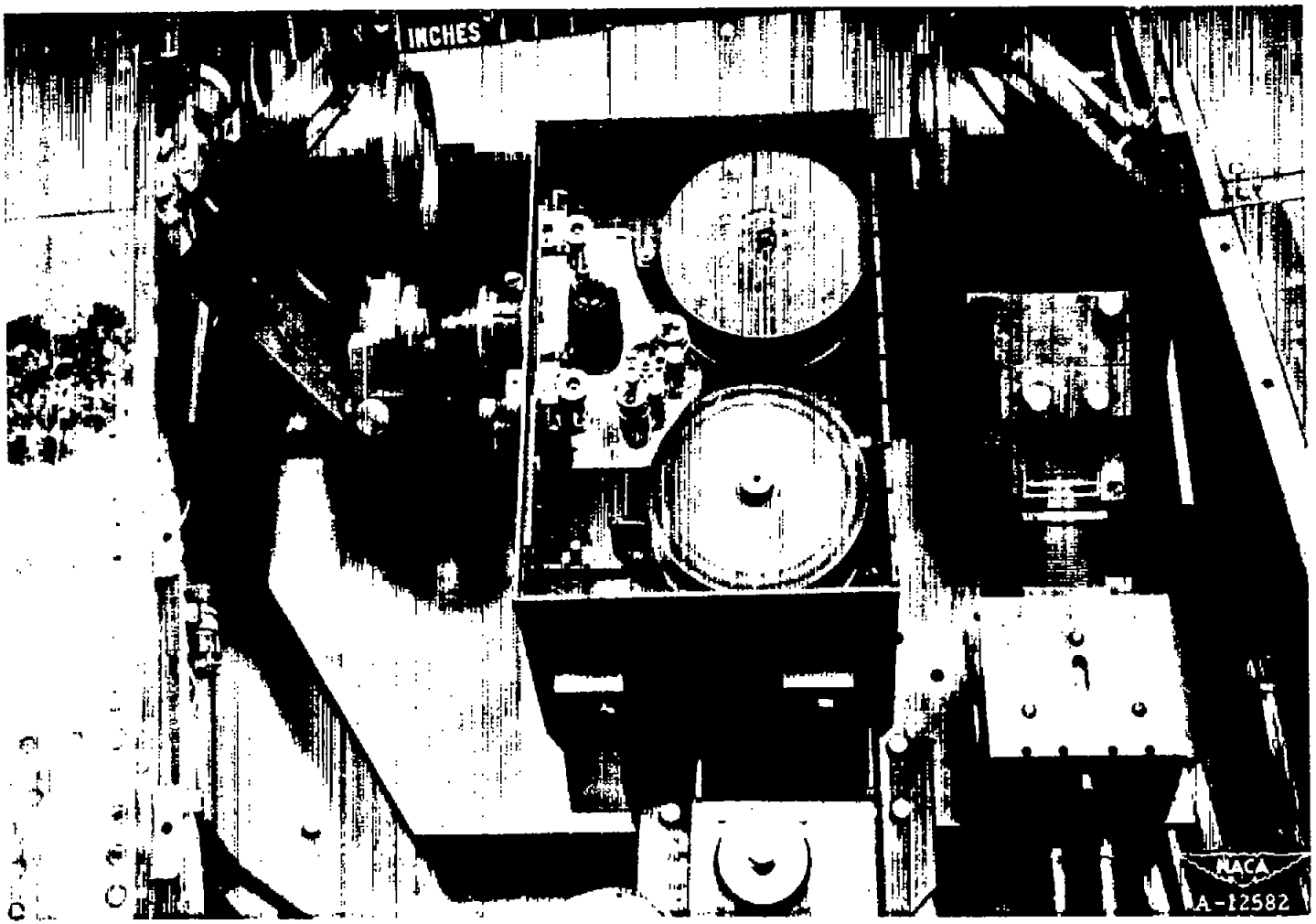

Figure 2.– Schlieren apparatus mounted in airplane wing.

Figure 3.- Left wing of test airplane with schlieren apparatus and fairings in place.

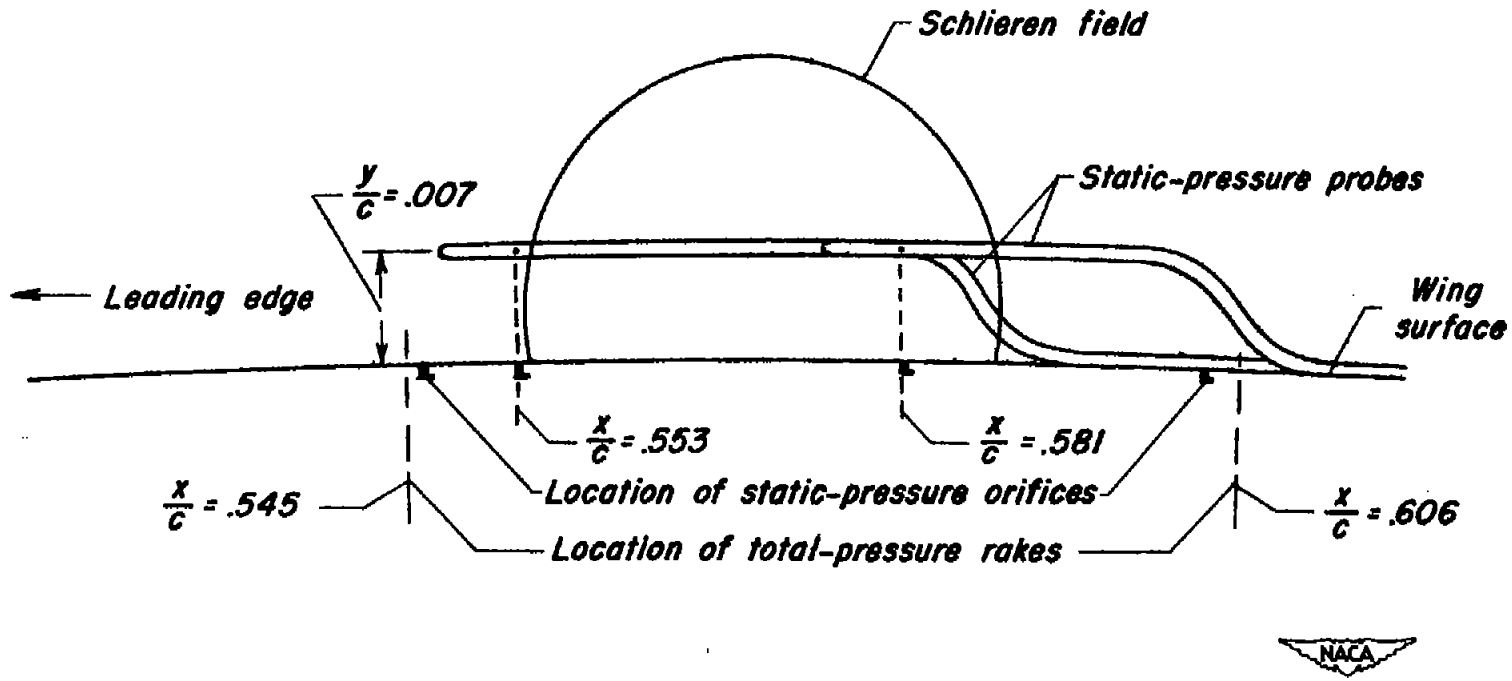

Figure 4.– Relative locations of schlieren field, surface orifices, static–pressure probes, and total–pressure rakes.

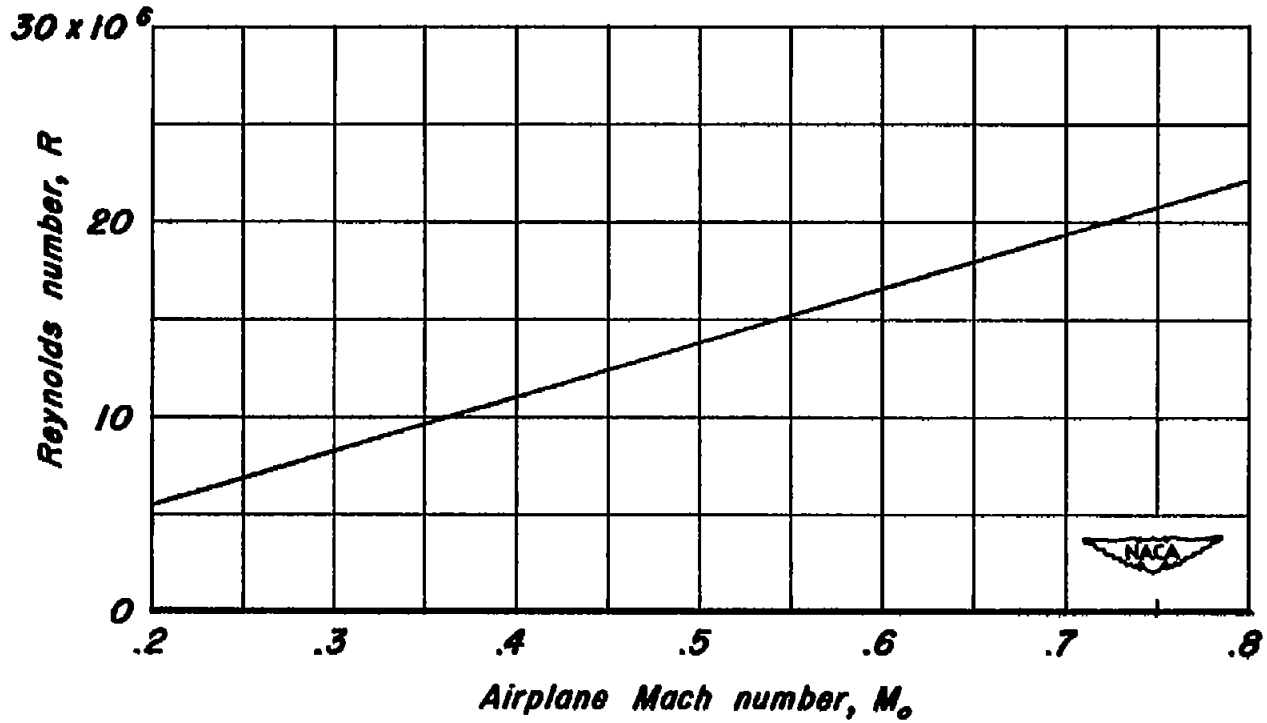

Figure 5.—Variation of Reynolds number with Mach number for the investigation.

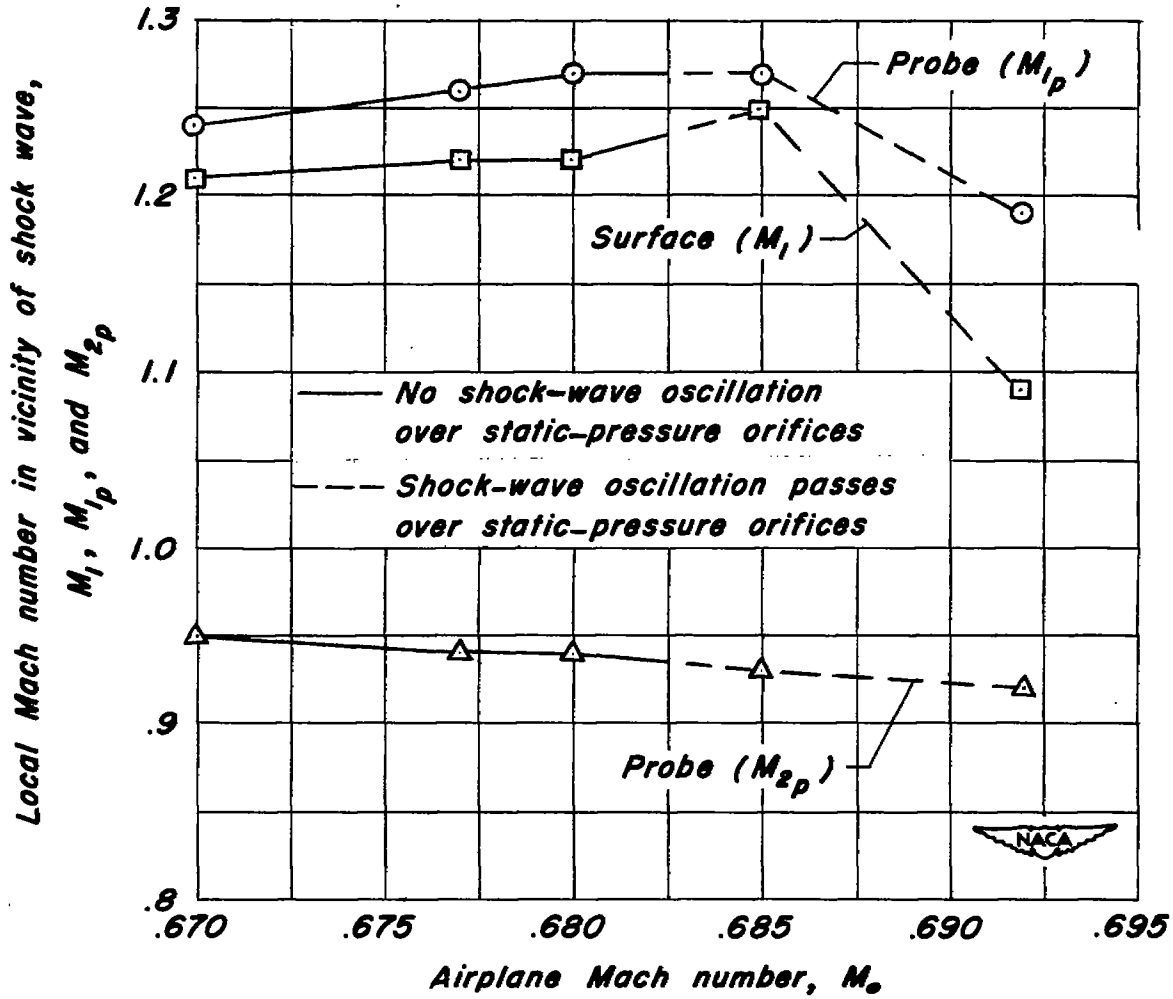

Figure 6.- Variation with airplane Mach number of local Mach number in the vicinity of the shock wave as determined from surface and probe static pressures.

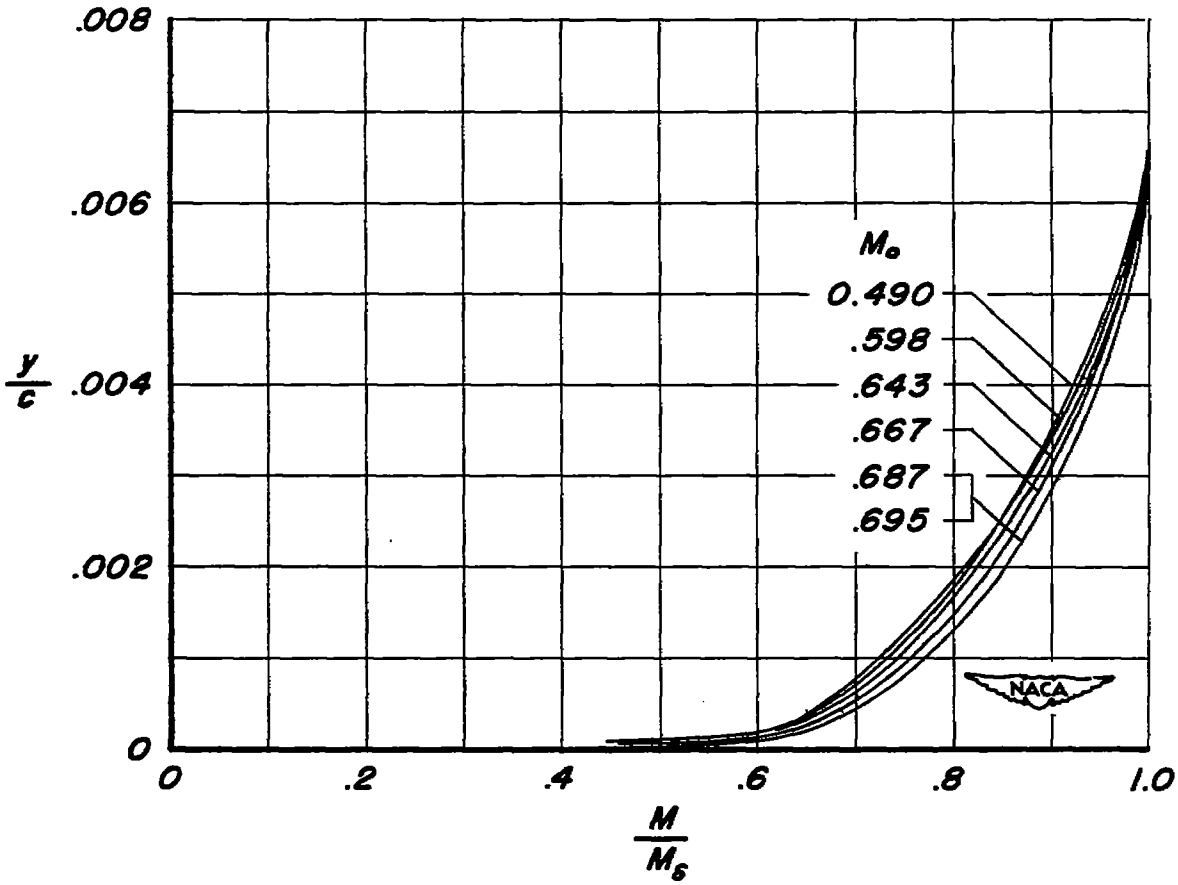

(a) $\frac{x}{c} = 0.545$

Figure 7.– Boundary–layer profiles .

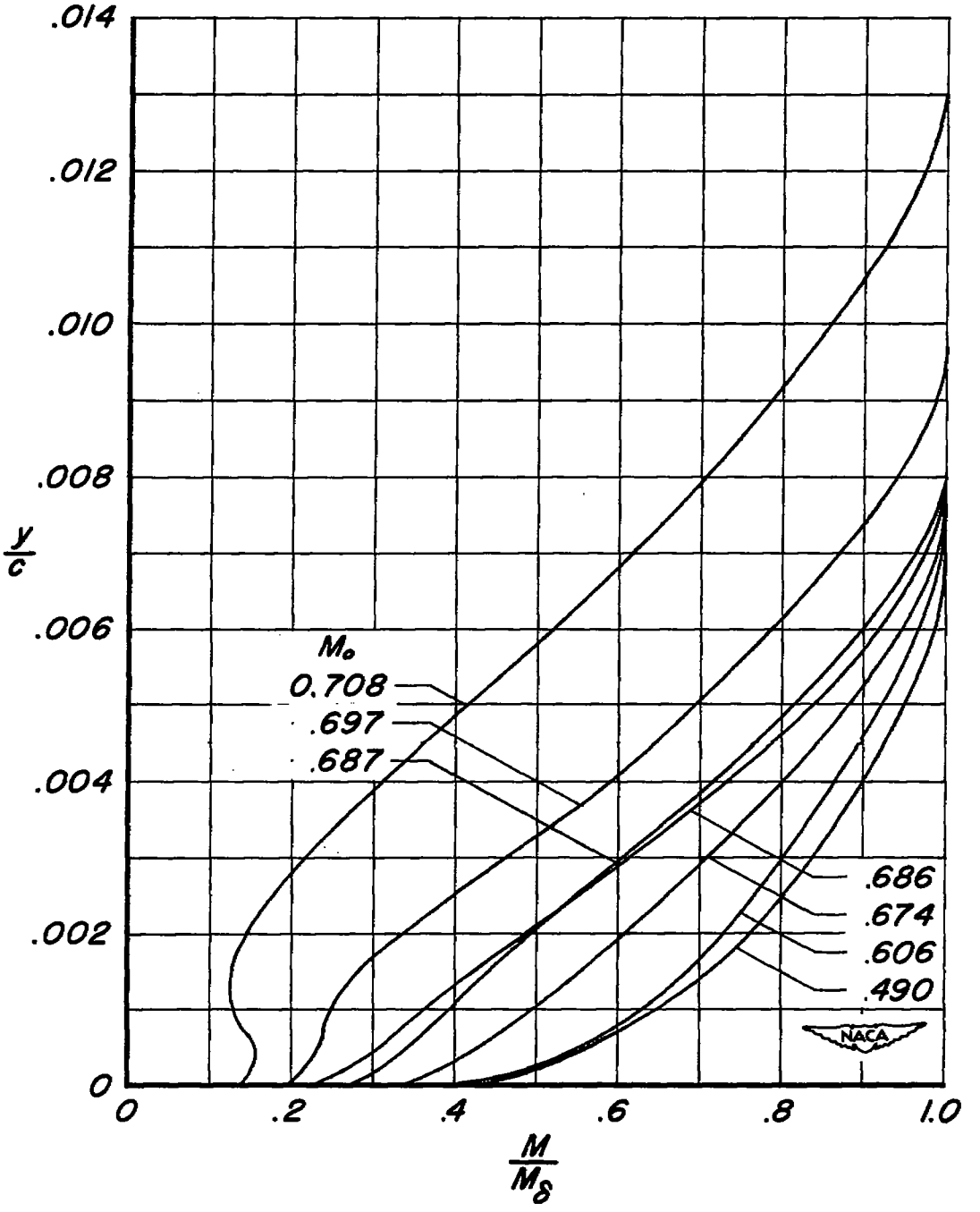

(b) $\frac{x}{c} = 0.606$

Figure 7.— Concluded.

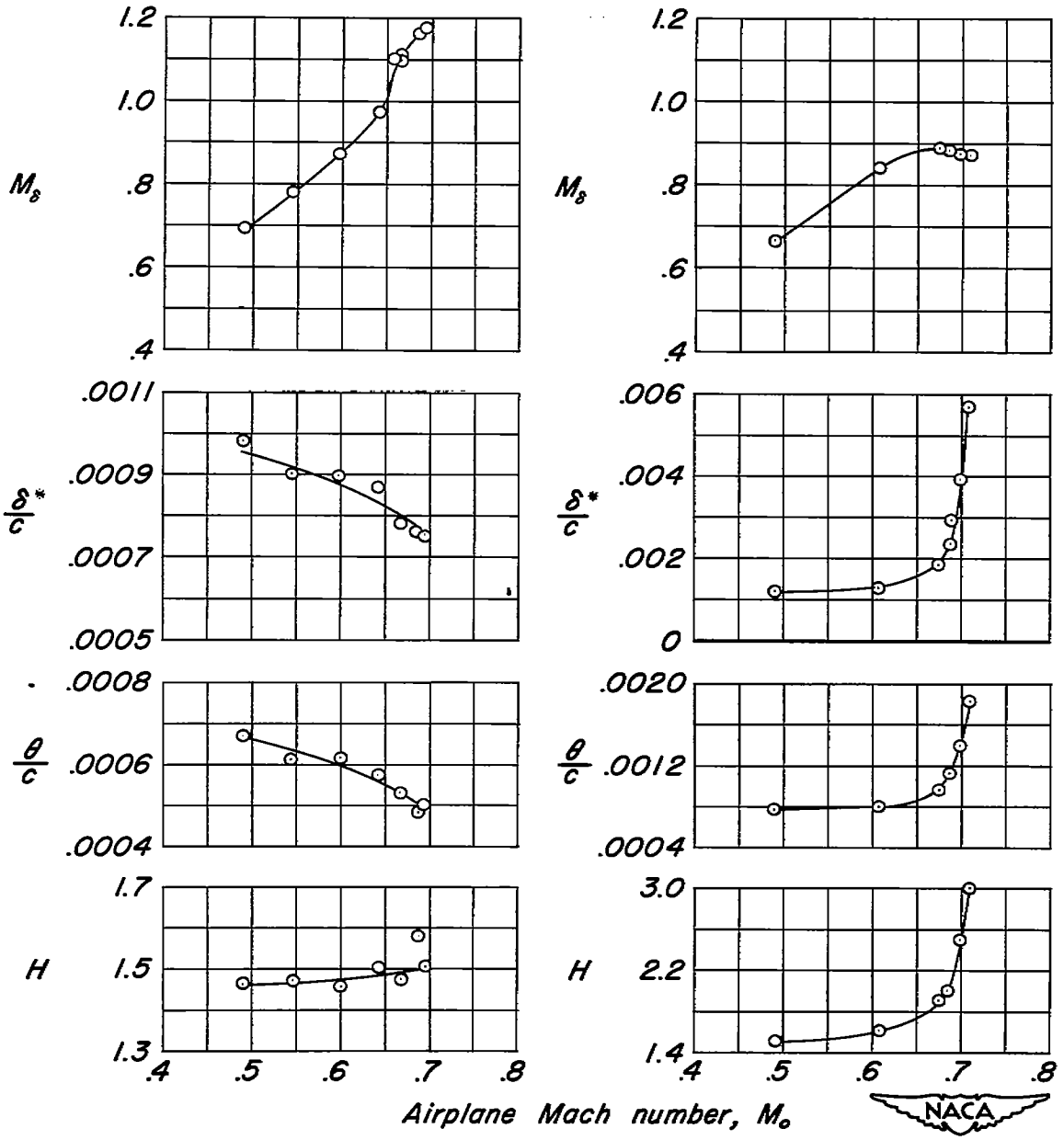

Figure 8.– Variation of M_s, $\frac{\delta^*}{c}$, $\frac{\theta}{c}$, and H with airplane Mach number.

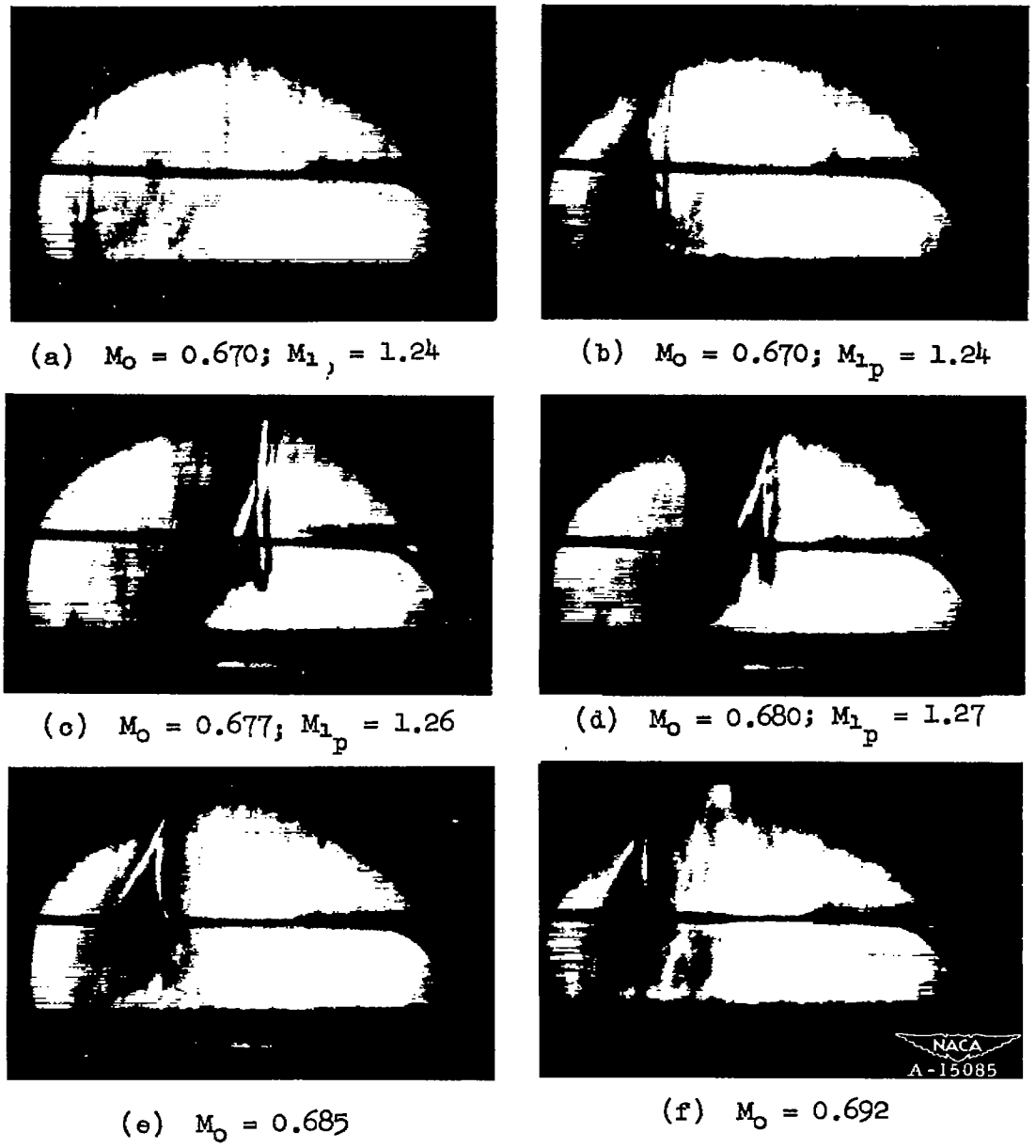

(a) $M_o = 0.670$; $M_{1_p} = 1.24$

(b) $M_o = 0.670$; $M_{1_p} = 1.24$

(c) $M_o = 0.677$; $M_{1_p} = 1.26$

(d) $M_o = 0.680$; $M_{1_p} = 1.27$

(e) $M_o = 0.685$

(f) $M_o = 0.692$

Figure 9.— Schlieren photographs of wing shock wave at various Mach numbers. (Nearly vertical cut-off.)

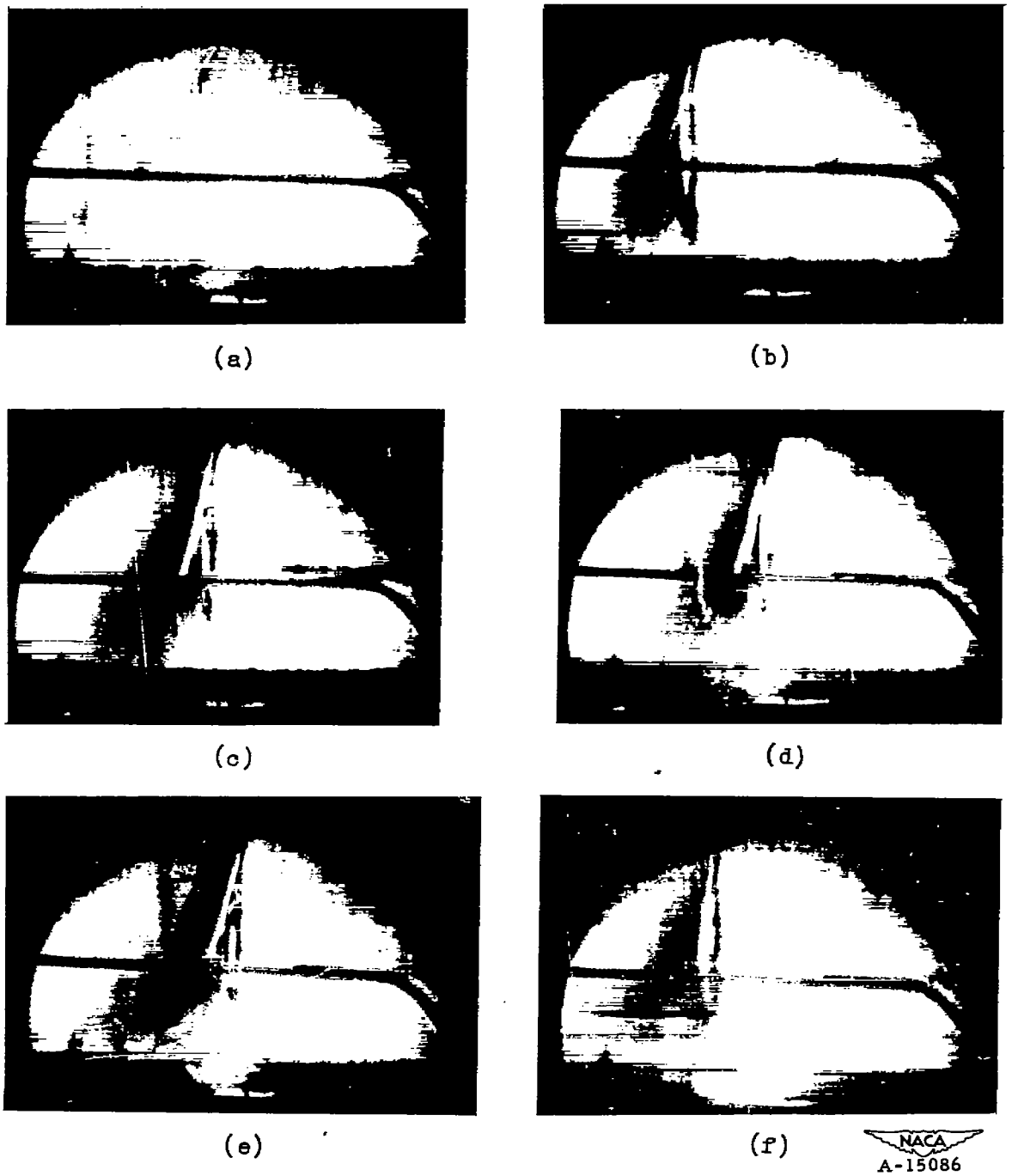

Figure 10.— A sequence of schlieren photographs showing transition from normal to forked shock wave for an airplane Mach number of 0.677, M_{1_p} = 1.26. (Nearly vertical cut-off.)

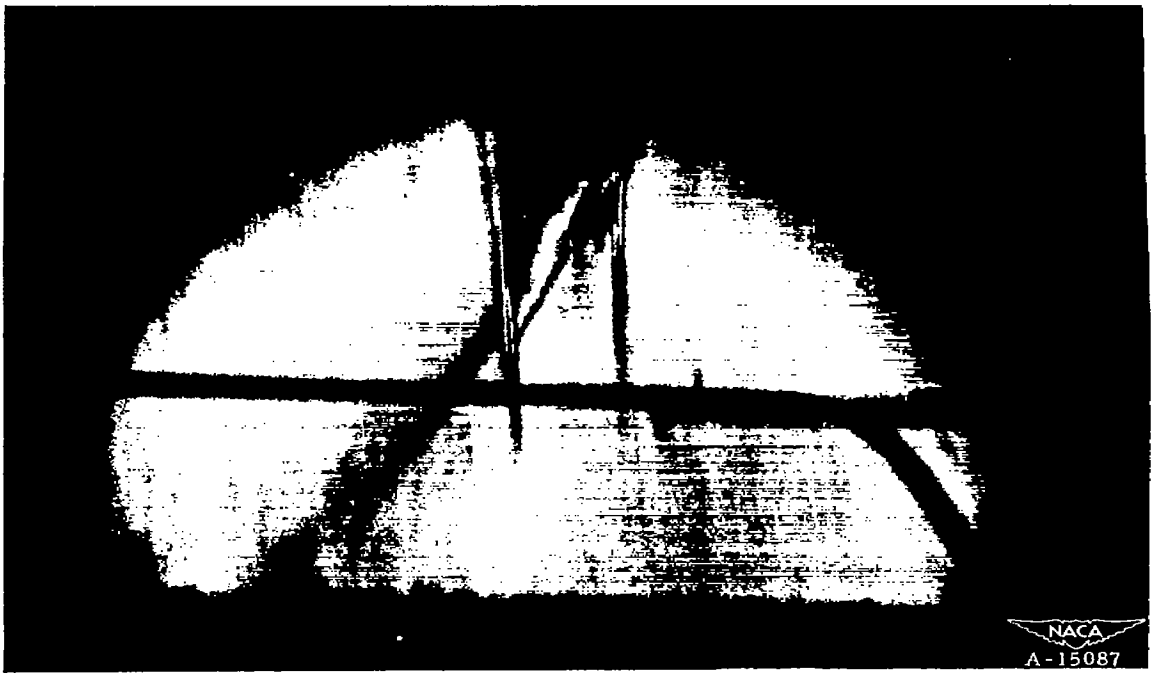

Figure 11.— Schlieren photograph of the forked shock wave obtained at an airplane Mach number of 0.685. (Nearly vertical cut-off.)

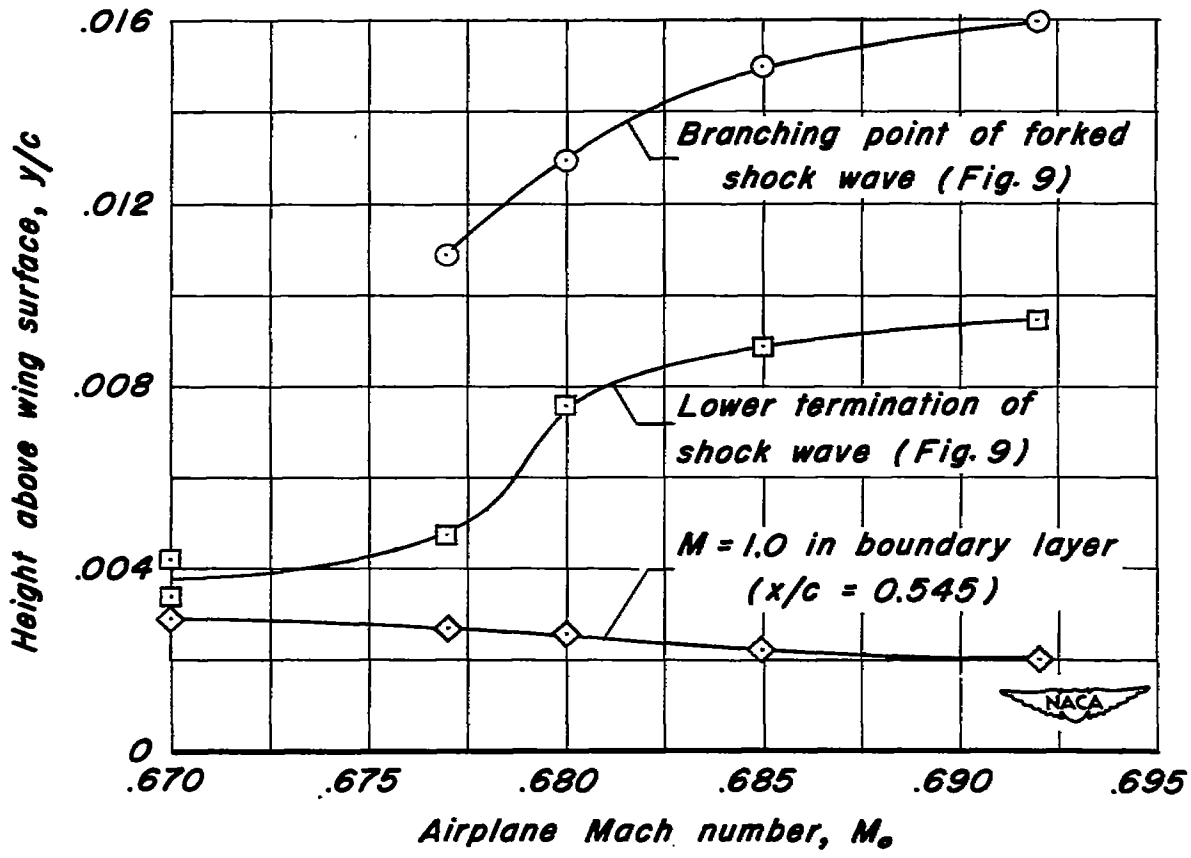

Figure 12.- Variation with airplane Mach number of the height of the shock-wave branching point and lower termination point, and the point in the boundary layer ahead of the shock where Mach number is unity.

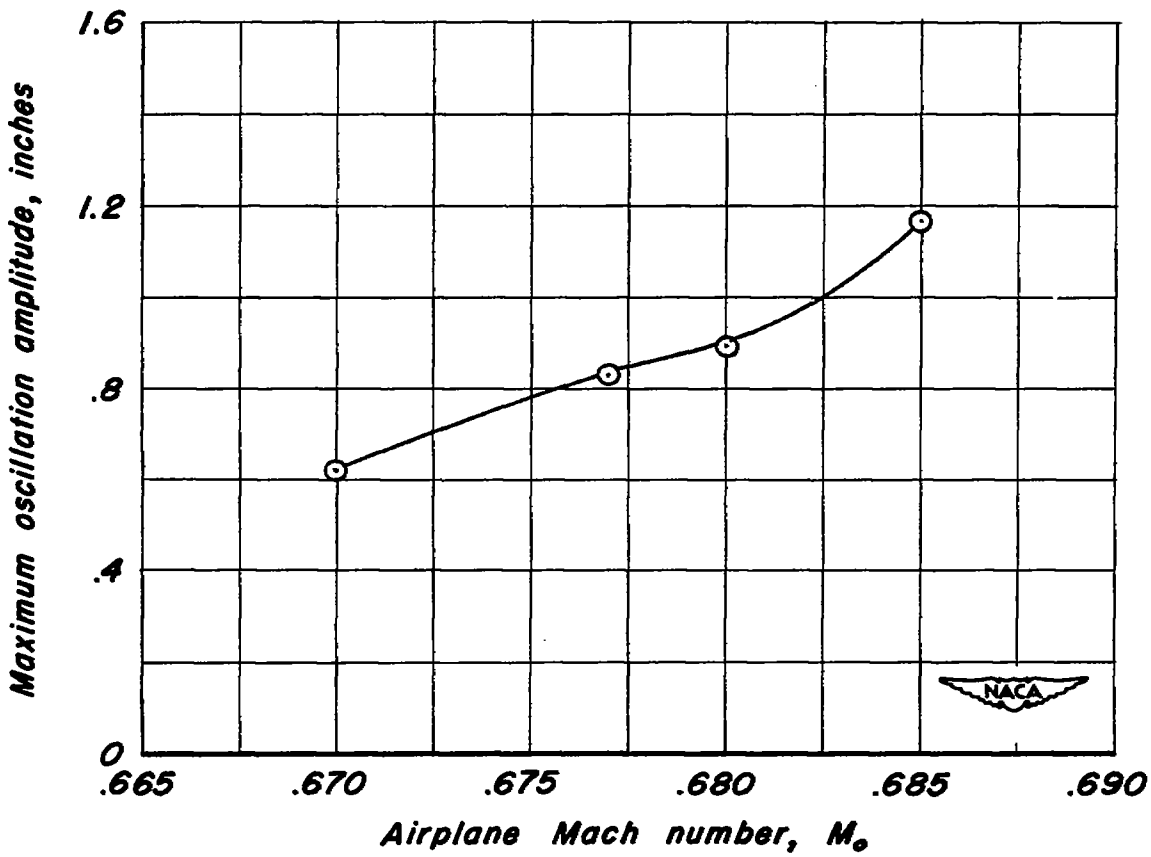

Figure 13.– Variation of maximum amplitude of shock-wave oscillation with airplane Mach number.

(a) $M_o = 0.605$; $M_1 = 0.90$

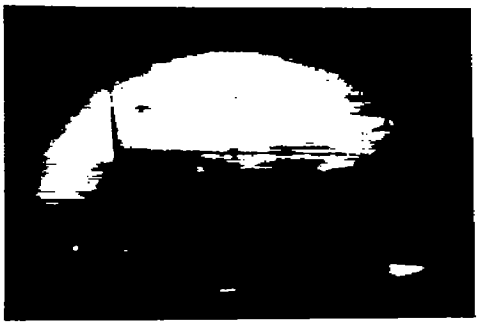

(b) $M_o = 0.673$; $M_1 = 1.21$

(c) $M_o = 0.675$; $M_1 = 1.22$

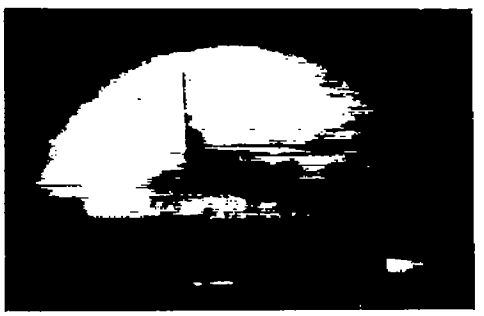

(d) $M_o = 0.680$; $M_1 = 1.22$

(e) $M_o = 0.684$

(f) $M_o = 0.690$

Figure 14.– Schlieren photographs of wing shock wave and/or boundary-layer at various Mach numbers. (Horizontal cut-off.)

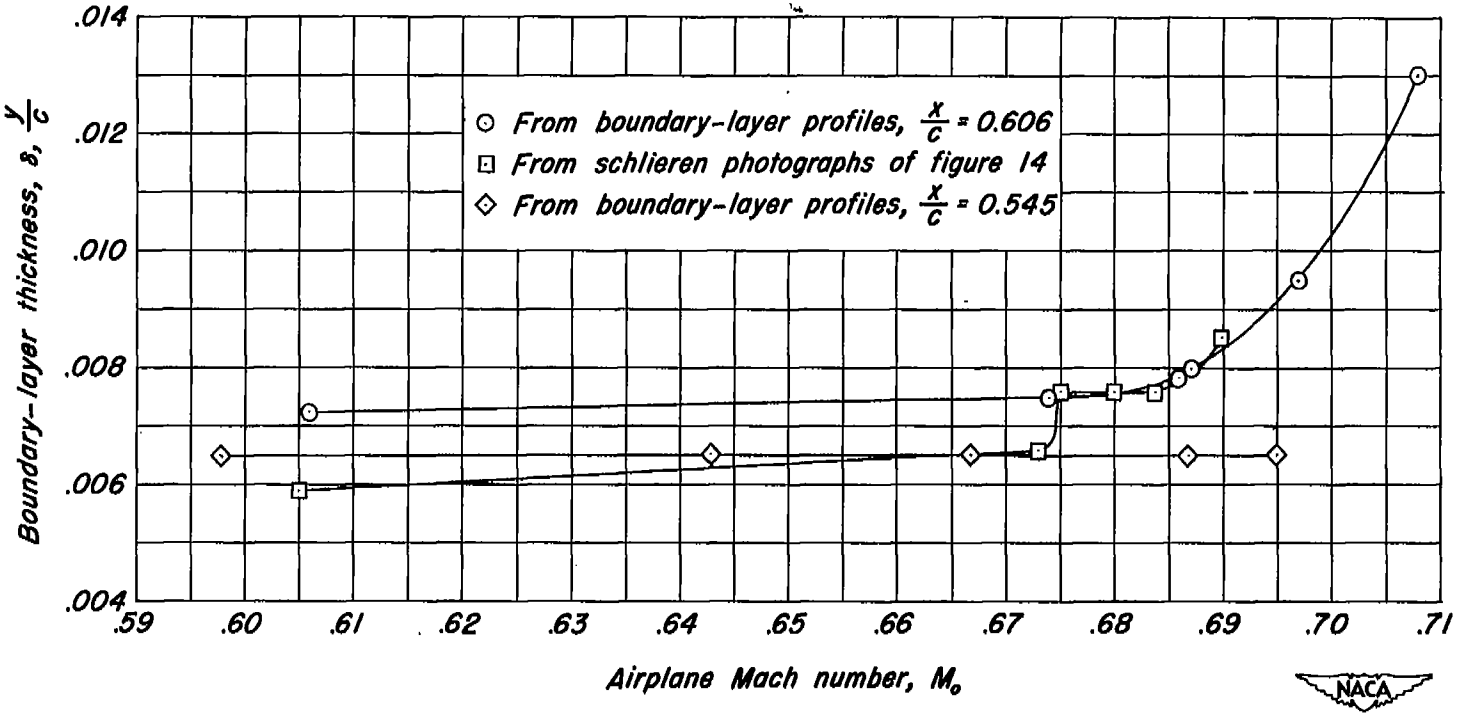

Figure 15.- Variation with airplane Mach number of boundary-layer thickness, as determined from boundary-layer profiles and schlieren photographs.